Title: Nanopore formation in the cuticle of the insect olfactory sensillum

Authors: Toshiya Ando[1, †], Sayaka Sekine[1], Sachi Inagaki[1, †], Kazuyo Misaki[1], Laurent Badel[3], Hiroyuki Moriya[4], Mustafa M. Sami[1], Takahiro Chihara[4, 5], Hokto Kazama[3], Shigenobu Yonemura[1], Shigeo Hayashi[1, 6, *]

Affiliations:

[1]RIKEN Center for Biosystems Dynamics Research, 2-2-3 Minatojima-minamimachi, Chuo-ku, Kobe, Hyogo 650-0047, Japan

[3]RIKEN Center for Brain Science, 2-1 Hirosawa, Wako, Saitama, 351-0198, Japan

[4]Department of Genetics, Graduate School of Pharmaceutical Sciences, The University of Tokyo, Hongo, Bunkyo-ku, Tokyo, Japan

[5]Department of Biological Science, Graduate School of Science, Hiroshima University, Higashi-Hiroshima, Hiroshima 739-8526, Japan

[6]Department of Biology, Kobe University Graduate School of Science, Kobe, Hyogo 657-8501, Japan.

*Correspondence to: shigeo.hayashi@riken.jp

[†]Present address: TA: National Institute of Basic Biology, Nishigonaka 38, Myodaijicho, Okazaki, Aichi, 444-8585, Japan, SI: Biosignal Research Center, Kobe University, 1-1 Rokkodai, Nada, Kobe 657-8501, Japan.

Short Title: Nano-level surface fabrication of apical ECM

Abstract: Insects sense odorants through small (50-200-nm diameter) pores in the cuticle covering the olfactory sensilla. These nanopores serve as a filter, preventing the entry of larger airborne particles and limiting water loss. Here we show that the nanopores in *Drosophila* originate from a curved ultrathin film formed in the outermost layer of the cuticle, secreted from specialized plasma membrane protrusions. The *gore-tex/Osiris23* gene, encoding an endosomal protein, is required for nanopore formation and odor receptivity, and is expressed specifically in developing olfactory shaft cells. The 24-member *Osiris* gene family is expressed in various cuticle-secreting cells, and is found only in insect genomes. Some *Osiris* mutants show defective cuticle-associated functions, suggesting that *Osiris* genes may provide a platform for investigating functional surface nano-fabrication in insects.

One Sentence Summary (125 characters)**:** An insect-specific endosomal protein promotes the formation of nano-scale pore structures of the apical extracellular matrix.

Main Text: The great success of insects in spreading throughout nearly the entire terrestrial ecosystem has been largely due to their exoskeleton, which enabled both their adaptation to harsh environments and protection from predators. The development of olfaction was also key in

helping insects search for food, mates, and other environmental cues, and to establish social communications (*1*). The insect olfactory sensillum consists of neurons that extend dendrites covered with exoskeletal sheaths. For volatile odorants to reach the dendrites, numerous pores ranging in diameter from 50 to 200 nm are formed in regular arrays on the cuticles of the olfactory sensory organs (*2*). Beneath the pores, membranous filaments called pore tubules extend to the interior lymph and dendritic nerve endings (*3*). These nano-scale structures are thought to allow the diffusion of small odorant molecules (0.5 to 5 nm in diameter) to reach the olfactory neurons, while preventing the entry of larger (100 to 1000 nm) airborne particles and minimizing the loss of inner lymph liquid. This selective filter system protects the olfactory neurons, which are not replaced throughout the adult life, from chemical and infectious damage. The molecular mechanisms determining the size and spatial patterns of nanopores, and how they are formed during cuticular scaffold assembly, are poorly understood. To elucidate the biological processes leading to this nanometer-order fabrication of extracellular matrix, here we investigated the molecular mechanisms of olfactory nanopore formation in the fruit fly *Drosophila melanogaster*.

Among the olfactory sensilla on the antennae and maxillary palps of *Drosophila* (Fig. 1A), we focused on those of the maxillary palp because of its simple structural composition: all ~60 of the olfactory sensilla deployed on a maxillary palp are morphologically categorized as middle length-type sensilla called basiconic sensilla (*6*, *8*). To understand when and how the pores are formed, we studied the process of cuticle secretion in olfactory hair cells using transmission electron microscopy (TEM). On the surface of these sensilla, pores of about 50-nm diameter are distributed along the long axis at 150- to 170-nm intervals (Fig. 1B, E). These sensilla form during pupal development from sensory organ precursor (SOP) cells, which give rise to multiple SOP-cell subtypes through several rounds of asymmetric cell division (*9*). Of these SOP-cell subtypes, a single cell called a shaft cell extends a cell protrusion covered with actin filaments toward the outside of the epithelium (Fig. 1F, 44 h APF [after puparium formation], green arrowheads). Then, the olfactory neurons project dendrites into the olfactory sensillum sheath (Fig. 1F, 52 h APF). At 74 h APF, the cellular projection of the shaft cell shrinks. The resulting shaft has dendrites filling its inner space and is covered with a chitin-rich cuticular sheath (Fig. 1G, 74 h APF). Adjacent to the olfactory sensilla, highly actin-rich hair cells (spinules), which lack neurites, undergo a similar extension process (Fig. 1C, Fig. 1F, magenta arrowhead).

Insect cuticles are organized in a layered structure consisting of an envelope, epicuticle, and chitin-rich procuticle, which are secreted in a step-wise manner (*10*). The first sign of envelope formation in the olfactory sensilla was observed at ~41 h APF as the appearance of electron-dense protrusions, similar to previously described plasma membrane plaques (PMPs) (*11*) the undule (*12*, *13*), or pimples (*14*) (Fig. 1G, 41 h APF). Above the PMP-positive cell surface at this stage, no distinct extracellular structure was observed (Fig. 1G, 41 h APF). Within the next few hours, each PMP was covered with diffuse material that acquired a solid appearance (Fig. 1H, J). This material eventually became the thin film of trilamellar envelope structures, and the PMP disappeared (Fig. 1D, Fig. 1G, 44, 46 h APF). PMPs appeared asynchronously over the surface of the olfactory shaft cells (Fig. 1H), and the envelope initially appeared as fragments (Fig. 1K). The piece-by-piece formation of envelope from fragments was also observed in adjacent hair cells (Fig. 1K), as previously described for the cuticles of *Drosophila* wing hair cells (*12*, *14*) and larvae (*13*), which form seamless cuticles. These observations imply that the PMPs function as a scaffold for the envelope-layer formation in olfactory shaft cells. Remarkably, the initial envelope pieces on the olfactory shaft cells were convex in shape, in contrast to the straight

appearance of the spinule cells (Fig. 1D, arrowhead). The convex envelope pieces were connected together with diffuse materials at their lowest point (Fig. 1K, yellow arrows). The cuticles had a wavy appearance in both longitudinal and transversal sections of the olfactory shaft cells at 52 h APF (Fig. 1L), and 3D reconstruction of the nascent envelope layer using serial block face-scanning electron microscopy (SBF-SEM) revealed numerous indentations with similar sizes and patterns as the pores on the surface of the adult olfactory sensillum (Fig. 1M), suggesting that the curved ultrathin envelope layer forms the nanopores at 52 h APF.

Olfactory hair cells at 44 h APF are rich in various membrane structures, including clathrin-coated vesicles (ccv) of about 50-nm diameter and clathrin-coated pits (ccp, Fig. 1I) that appear near the plasma membrane. Image analyses revealed that 84% of the ccv (N=31) and 77% of the ccp (N=13) were located between neighboring PMPs or envelope fragments. In contrast, in the spinule cells at 44 to 46 h AFP, vesicle structures were rarely observed near the plasma membrane, where dense arrays of actin filaments occupied the space (Fig. 1D, K).

At 52 h APF, electron-dense extracellular structures appeared at the lowest point of the wavy envelope layer (Fig. 1G, 52 h APF, orange arrowheads). These structures were aligned at 150- to 200-nm intervals in sagittal sections (Fig. 1L, left) and in horizontal sections (Fig. 1L, right). Three-dimensional imaging by electron tomography revealed complex folded structures associated with the envelope layer (Fig. 1N, movie S1). These structures, which were detergent sensitive (Fig. S1), disappeared after 64 h APF and were replaced by cloudy material beneath the nascent pore structures that persisted after the shaft cell retraction (74 h APF, orange arrowheads). It is possible that the lamellar structures are the material for the pore tubule that is thought to serve as a channel for the delivery of odorant molecules to the dendrites of the olfactory neurons (*5*, *15*).

These TEM studies suggested that a specialized cellular process for apical extracellular matrix (aECM) assembly must be present in the olfactory shaft cells to produce the curved envelope pieces and nanopores. To identify the molecular components specifying the nanopores, we made the assumption that the putative nanopore-formation genes must fulfil the following criteria: 1) expressed in olfactory shaft cells at the time of shaft cell envelope formation (2 days APF), 2) but not expressed in the pore-less mechanosensory hair cells or neuronal cells, and 3) encode membrane-associated proteins. We then performed RNA-seq analysis focusing on two genetic conditions: one that transforms shaft cells to neurons [overexpression of *numb*, (*16*)] and the other that converts olfactory sensory organs into mechanosensory organs [*amos* mutants, (*17*)]. Pupal antennae at 52 h APF were collected for analysis (Materials and Methods, Data S1). The RNA-seq profiles of the above two genetic conditions were compared with that of wild type in triplicate samplings, and transcripts that were downregulated in the mutants were further filtered for the presence of a signal peptide and transmembrane domains. Twenty-six candidate genes selected from this screen were then knocked down in developing olfactory shaft cells by a transgenic RNAi method, and the olfactory sensillum morphology in the maxillary palp was observed by field emission scanning electron microscopy (FE-SEM). Among the 30 RNAi strains tested, two caused a loss of the nanopore phenotype (Fig. 2A, B). These two RNAi strains were targeted to the same gene (CG15538), which was named *gore-tex (gox)*. According to the developmental RNA-seq profile in the modENCODE database, the *gox* transcript is detected only in 2-day-old pupae (*18*). Two *gox* mutations created by genome editing (Fig. S2) were homozygous viable and fertile, with no visible defect in adult external morphology at the macroscopic level. However, high-resolution helium ion microscopy (HIM) of the olfactory

sensilla revealed a significant loss of nanopores, and this phenotype was partially rescued by the overexpression of *gox* (Fig. 2A, B). Recording of the local field potential in maxillary palps revealed that the loss of *gox* by mutations or RNAi greatly reduced the responses to both strong (a mixture of odors that strongly activate sensory neurons in the palp) and weak (milder solvent) odor stimuli (Fig. 2C, D). TEM analysis of 52 h APF gox^1 mutant olfactory sensilla exhibited a flat cuticular envelope and no pore structures, suggesting that the *gox* function is required to introduce curvature into the newly formed envelope fragments, prior to nanopore formation (Fig. 2E).

The predicted Gox protein contains an N-terminal signal peptide, two copies of a putative transmembrane domain, and a domain with similarity to a sequence called "protein of unknown function" (DUF1676) found in insect genomes (Fig. 3A). The presence of two transmembrane domains is unconventional. To determine the topology of the Gox protein relative to the membrane, we analyzed the locations of its N-terminal and C-terminal regions using the split GFP tagging method, and found that Gox extends its C-terminus into the cytoplasm and its N terminus into the lumen of intracellular vesicles or the extracellular space (Fig. S3A). Gox protein expressed in *Drosophila* S2 cells was co-localized with HRS (early endosome marker) and Rab7 (late endosome marker), but not with an endoplasmic reticulum marker Calnexin (Fig. S3B). An HA-tagged *gox* genomic construct showed Gox expression in the shaft cells of olfactory sensillum, but not in spinules (Fig. 3B, B'), and not in neurons (Fig. 3B''). Super-resolution imaging revealed that HA-Gox was localized to intracellular vesicles that overlapped with HRS and Rab7 (Fig. 3C). These results indicated that Gox is a transmembrane protein that mainly localizes to the endosomes of shaft cells of olfactory sensillum.

The *gox* gene belongs to a 24-member gene family called *Osiris (Osi)*. Of the 24 *Osiris* genes, 21 are clustered at position 83E of chromosome 3R, and are included in a locus that exhibits a rare dosage sensitivity (triplo-lethal and haplo-lethal) (*19*, *20*). The other three are located at 32E (*Osi21*), 87E (*Osi22*), and 99F (*gox/Osi23*). To obtain information about the function of *Osiris* genes, we investigated the mRNA expression of 24 *Osiris* genes in *Drosophila* embryos by *in situ* hybridization. We found that all of the *Osi* genes were expressed at variable levels and patterns in late embryonic stages when the cuticle is secreted, in various tissues, including the epidermis, mouth parts, foregut, hindgut, trachea, and spiracles (Fig. 4A, Table S1, Data S2, supplementary text). We classified the *Osiris* expression patterns into 8 types, which collectively covered essentially all of the cuticle-producing organs of first-instar larvae (Fig. S4). Of these mRNAs, *Osi6* and *Osi7* were expressed broadly in the epidermis and head skeleton. When *Osi6* and *Osi7* were knocked out by genome editing, the resulting heterozygous animals were weak and sluggish, and homozygous animals were embryonic lethal, with poor formation of the cepharo-pharyngeal skeleton and denticle belts (Fig. 4B, C). Homozygous *Osiris19* mutants were semi-lethal and showed a loss of ocelli and a rough-eye phenotype (Fig. 4D). These results collectively indicated that *Osiris* genes are expressed mainly in cuticle-secreting epidermal tissues at cuticle-secretion stages, and that the available null mutations of four of them (*Osi6, Osi7, Osi19,* and *gox/Osi23*) caused various defects in cuticle patterning or functions, as previously suggested from bioinformatics analysis (*21*).

Osiris gene families with DUF1676 domain have been found in a number of insect genomes, but not in the genome of other animal classes including Crustaceans, Myriapod, Chelicerata and Entognatha (Collembola) (*22*)(*21*), suggesting that this gene family was acquired at an early stage of insect genome evolution, when crustacean-like insect ancestors changed their habitat from an aquatic to a terrestrial environment and expanded their niche (*23*). This finding leads to

an interesting hypothesis that the acquisition of *gore-tex/Osiris23* drove the change in olfactory sensillum structure from the thin, permeable cuticles of crustaceans to the porous structures of insects (*24*). How the Gore-tex protein, which is localized to endosomal compartments, affects the extracellular events of cuticle envelope assembly is still unclear. One possibility is that Gore-tex regulates the trafficking of specific effector molecules for cuticle assembly, as previously suggested for the function of *Osi21/die4* in regulating endocytosed rhodopsin in photoreceptor cells (*25*). Alternatively, gore-tex protein may help to pattern the endocytosis of the olfactory shaft cell membrane. It is notable that the spacing and alignment pattern of the nanopores is highly regular, coinciding to the position of ccp and ccv adjacent to the PMPs at ~44 h APF. Targeting the site of endocytosis between PMPs would enhance the periodicity of endocytic and exocytic activities, leading to cuticle undulation, as previously suggested for the taenidial fold formation in the *Drosophila* trachea (*26*). The nano-scale surface patterning of extracellular matrices forms the basis for the vast variety of functional biological surfaces with specific properties of, for example, structural color, water repellency, and light absorption (*27-29*). Further studies of *gore-tex/Osiris23* and its family members should uncover mechanisms behind the specialized features of biological nano-patterning in the aECM.

References and Notes:

1. K.-E. Kaissling, in *Olfaction* (Springer, Berlin, Heidelberg, Berlin, Heidelberg, 1971), vol. 4 of *Handbook of Sensory Physiology*, pp. 351–431.

2. A. G. Richards, Studies on arthropode cuticle. VIII. The antennal cuticle of honeybees, with particular reference to the sense plates. *The Biological Bulletin*. **103**, 201–225 (1952).

3. E. H. Slifer, The permeability of the sensory pegs on the antennae of the grasshopper (Orthoptera, Acrididae). *The Biological Bulletin*. **106**, 122–128 (1954).

4. D. Schneider, Insect Olfaction: Deciphering System for Chemical Messages. *Science*. **163**, 1031–1037 (1969).

5. R. A. Steinbrecht, Pore structures in insect olfactory sensilla: A review of data and concepts. *International Journal of Insect Morphology and Embryology*. **26**, 229–245 (1997).

6. S. R. Shanbhag, B. Muller, R. A. Steinbrecht, Atlas of olfactory organs of Drosophila melanogaster 1. Types, external organization, innervation and distribution of olfactory sensilla. *International Journal of Insect Morphology and Embryology*. **28**, 377–397 (1999).

7. S. R. Shanbhag, B. Muller, R. A. Steinbrecht, Atlas of olfactory organs of Drosophila melanogaster 2. Internal organization and cellular architecture of olfactory sensilla. *Arthropod Structure & Development*. **29**, 211–229 (2000).

8. M. de Bruyne, P. J. Clyne, J. R. Carlson, Odor Coding in a Model Olfactory Organ: The Drosophila Maxillary Palp. *Journal of Neuroscience.* **19**, 4520–4532 (1999).

9. K. Endo, T. Aoki, Y. Yoda, K.-I. Kimura, C. Hama, Notch signal organizes the Drosophila olfactory circuitry by diversifying the sensory neuronal lineages. *Nat Neurosci*. **10**, 153–160 (2007).

10. V. B. Wigglesworth, The insect cuticle. *Biological Reviews*. **23**, 408–451 (1948).

11. M. Locke, P. Huie, Apolysis and the turnover of plasma membrane plaques during cuticle formation in an insect. *Tissue And Cell.* **11**, 277–291 (1979).

12. L. F. Sobala, P. N. Adler, The Gene Expression Program for the Formation of Wing Cuticle in Drosophila. *PLoS Genet*. **12**, e1006100 (2016).

13. B. Moussian, C. Seifarth, U. Müller, J. Berger, H. Schwarz, Cuticle differentiation during Drosophila embryogenesis. *Arthropod Structure & Development*. **35**, 137–152 (2006).

14. G. M. Guild, P. S. Connelly, L. Ruggiero, K. A. Vranich, L. G. Tilney, Actin filament bundles in Drosophila wing hairs: hairs and bristles use different strategies for assembly. *Mol Biol Cell*. **16**, 3620–3631 (2005).

15. M. Locke, Permeability of Insect Cuticle to Water and Lipids. *Science*. **147**, 295–298 (1965).

16. M. S. Rhyu, L. Y. Jan, Y. N. Jan, Asymmetric distribution of numb protein during division of the sensory organ precursor cell confers distinct fates to daughter cells. *Cell*. **76**, 477–491 (1994).

17. P. I. zur Lage, D. R. A. Prentice, E. E. Holohan, A. P. Jarman, The Drosophila proneural gene amos promotes olfactory sensillum formation and suppresses bristle formation. *Development*. **130**, 4683–4693 (2003).

18. http://flybase.org/cgi-bin/rnaseqmapper.pl?dataset=tissues_stranded&xfield1=FBgn0039771

19. D. L. Lindsley *et al.*, Segmental aneuploidy and the genetic gross structure of the Drosophila genome. *Genetics*. **71**, 157–184 (1972).

20. D. R. Dorer, J. A. Rudnick, E. N. Moriyama, A. C. Christensen, A family of genes clustered at the Triplo-lethal locus of Drosophila melanogaster has an unusual evolutionary history and significant synteny with Anopheles gambiae. *Genetics*. **165**, 613–621 (2003).

21. C. R. Smith, C. Morandin, M. Noureddine, S. Pant, Conserved roles of Osiris genes in insect development, polymorphism and protection. *Journal of Evolutionary Biology*. **31**, 516–529 (2018).

22. N. Shah, D. R. Dorer, E. N. Moriyama, A. C. Christensen, Evolution of a large, conserved, and syntenic gene family in insects. *G3: Genes|Genomes|Genetics*. **2**, 313–319 (2012).

23. G. Giribet, G. D. Edgecombe, Reevaluating the Arthropod Tree of Life. *Annual Review Of Entomology*. **57**, 167–186 (2012).

24. C. D. Derby, M. T. Kozma, A. Senatore, M. Schmidt, Molecular Mechanisms of Reception and Perireception in Crustacean Chemoreception: A Comparative Review. *Chem Senses*. **41**, 381–398 (2016).

25. J. Lee, M. Song, S. Hong, Negative Regulation of the Novel norpAP24 Suppressor, diehard4, in the Endo-lysosomal Trafficking Underlies Photoreceptor Cell Degeneration. *PLoS Genet*. **9**, e1003559 (2013).

26. A. Öztürk-Çolak, B. Moussian, S. J. Araújo, J. Casanova, U. Banerjee, A feedback mechanism converts individual cell features into a supracellular ECM structure in Drosophila trachea. *eLife*. **5**, e09373 (2016).

27. W. Barthlott, C. Neinhuis, Purity of the sacred lotus, or escape from contamination in biological surfaces. *Planta*. **202**, 1–8 (1997).

28. M. D. Shawkey, N. I. Morehouse, P. Vukusic, A protean palette: colour materials and mixing in birds and butterflies. *Journal of The Royal Society Interface*. **6**, S221–S231 (2009).

29. D. G. Stavenga, S. Foletti, G. Palasantzas, K. Arikawa, Light on the moth-eye corneal nipple array of butterflies. *Proceedings of the Royal Society B: Biological Sciences*. **273**, 661–667 (2006).

Acknowledgments:

We thank Shigehiro Kuraku and his laboratory members at RIKEN BDR for technical support for the RNA-seq analysis; Carl Zeiss Japan, and Shinichi Ogawa (the National Institute of Advanced Industrial Science and Technology [AIST]) for the use of HIM; Atsushi Yamaguchi (Hyogo Prefectural Institute of Technology) for the use of FE-SEM; Andrew Jarman (The University of Edinburgh), Masayuki Miura (The University of Tokyo), the *Drosophila* stock centers of Kyoto, NIG, and Bloomington for fly stocks; the Developmental Studies Hybridoma Bank, Akira Nakamura (Kumamoto University), and Hugo Bellen (Baylor Colledge of Medicine) for antibodies; Hosei Wada (RIKEN BDR) for genome engineering support; Hiromi Niwa for illustration; and Mai Shibata (RIKEN BDR) for support for cell culture experiments. We are grateful to Masayuki Miura (The University of Tokyo) for supporting the project performed by H.M. and T.C., and Rudolf Alexander Steinbrecht (Max Planck Institute for Ornithology) for discussion. A part of this work (HIM) was conducted at the Nano-Processing Facility, supported by IBEC Innovation Platform, AIST. **Funding:** This study was supported by JSPS KAKENHI Grant Number 15K18811. **Author contributions:** T.A. and S.H. conceived of the project, and designed the experiments. T.A. performed the TEM analysis with K.M. and S.Y., and the electrophysiological analysis with L.B. and H.K. S.S. performed the cellular

localization analysis of *gox/Osi23* with the help of S.H., and created the *gox/Osi23* mutants. The other *Osi* mutants were created by H.M. and T.C. S.I. performed the *in situ* hybridization analysis. M.M.S. developed the tool for the image analysis. T.A. performed the other experiments, and analyzed the experimental data with the help of S.H. T.A and S.H. wrote the manuscript with the help of S.S. and H.K. **Competing interests:** Authors declare no competing interests. **Data and materials availability:** The materials used in this work are available for researchers (materials transfer agreements may be required). The RNA-seq data are deposited at Genbank under the accession number SRP155317.

Supplementary Materials:

Materials and Methods

Supplementary Text

Figs. S1 to S4

Tables S1

Caption for Movie S1

Captions for Data S1 to S4

References (*30-43*)

Figure 1

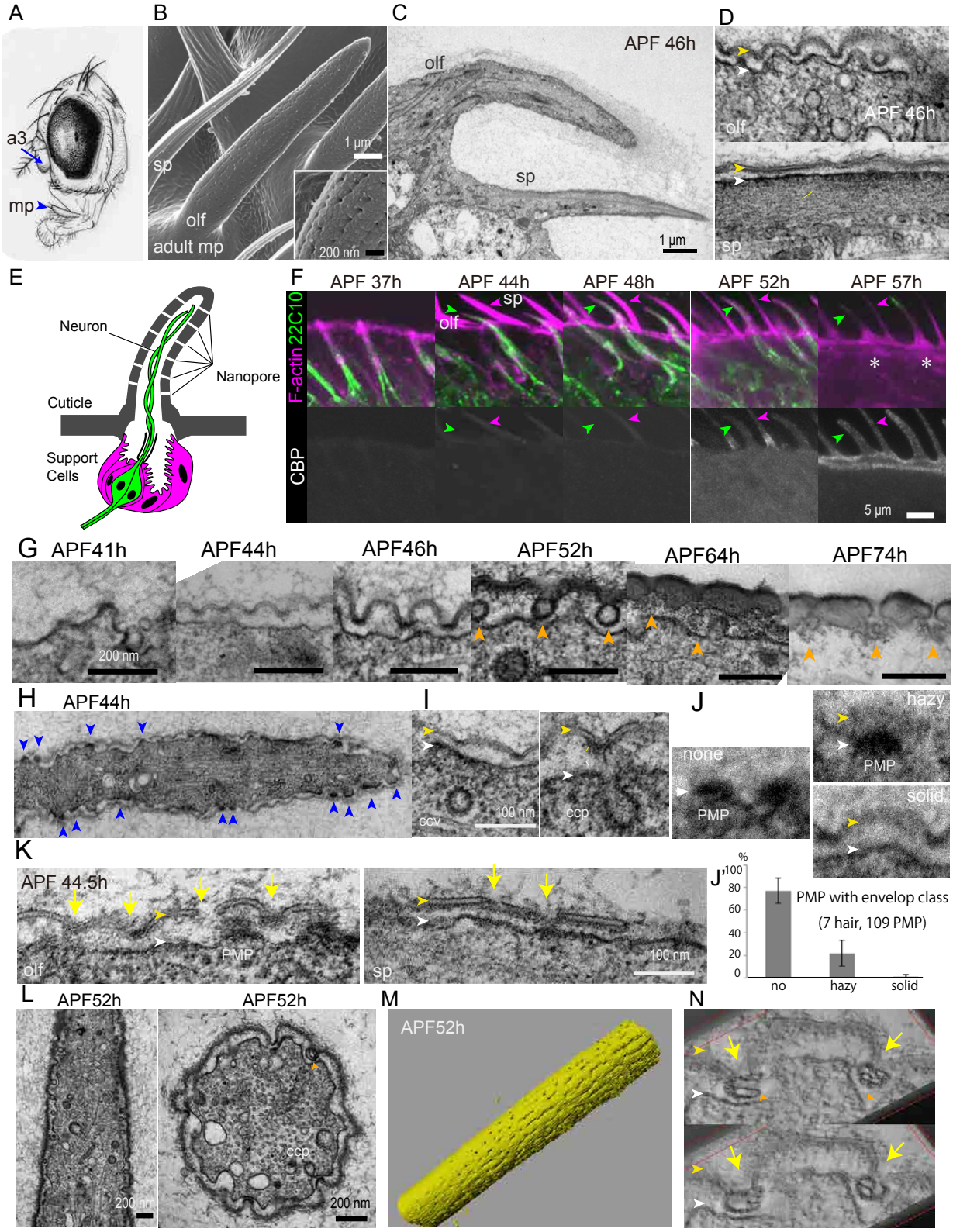
A
a3
mp
B
sp
olf
adult mp
1 µm
200 nm
C
APF 46h
olf
sp
1 µm
D
olf
APF 46h
sp
E
Neuron
Nanopore
Cuticle
Support
Cells
F
APF 37h
APF 44h
APF 48h
APF 52h
APF 57h
F-actin 22C10
CBP
sp
olf
5 µm
G
APF41h
APF44h
APF46h
APF52h
APF64h
APF74h
200 nm
H
APF44h
I
ccv
100 nm
ccp
J
none
PMP
hazy
PMP
solid
K
APF 44.5h
olf
PMP
sp
100 nm
J'
%
PMP with envelop class
(7 hair, 109 PMP)
no
hazy
solid
L
APF52h
APF52h
ccp
200 nm
200 nm
M
APF52h
N

Fig. 1. Development of olfactory nanopores. (A) Olfactory sensilla are present on the 3rd antennal segment (a3) and the maxillary palp (mp) of the adult head. (B) A surface image of adult maxillary palp showing olfactory sensilla (olf) and non-sensory spinule (sp). Inset shows regularly arranged nanopores. (C) A TEM image of olf and sp at 46 h APF. (D) Enlarged cross-sectional views of newly formed cuticular envelope (yellow arrowheads) and plasma membrane (white arrowheads). Note undulated envelope and plasma membrane with numerous intracellular and extracellular vesicles at the olf (top). In the sp, the envelope and plasma membrane were flat, and extensive actin filaments were associated with the plasma membrane (bottom). (D) Schematic of a porous olf. (E) Time course of olf and sp formation in mp stained for a neuronal marker (22C10, green), F-actin (magenta), and chitin (black and white panels). Neurons were associated with olf (green arrowhead), but not with sp (magenta arrowhead), which was enriched in F-actin. Chitin was secreted after 52 h APF, and restricted the internal staining of neurons (*) at 57 h APF. (G) Time course of cuticle nanopore formation. Orange arrowheads show vesicle-like envelope-associated structures at 52 h APF, and pore tubules at 64 h APF and later. Shaft cell retraction was complete at 74 h APF. (H) Overview of olf at 44 h APF with extensively undulated surfaces and sporadic PMPs (arrowheads). (I) Examples of clathrin-coated vesicle (ccv) and clathrin-coated pit (ccp) near the site of envelope formation. (J) Three steps of envelope formation (none, hazy, solid) and the frequency of PMPs associated with each class (J'). (K) An enlarged view of olf and sp cell surface associated with envelope pieces of regular size (yellow arrowheads) on top of plasma membrane (white arrowheads). Yellow arrows indicate connection points of envelope pieces. (L) Longitudinal and cross-sectional views of olf at 52 h APF, showing envelope curvature and an extracellular envelope-associated structure (orange arrowhead). (M) A reconstructed surface view of olf obtained by SBF-SEM. (N) Complex envelope-associated structures shown by electron tomography. Top and bottom images show the same specimen viewed from different angles.

Figure 2

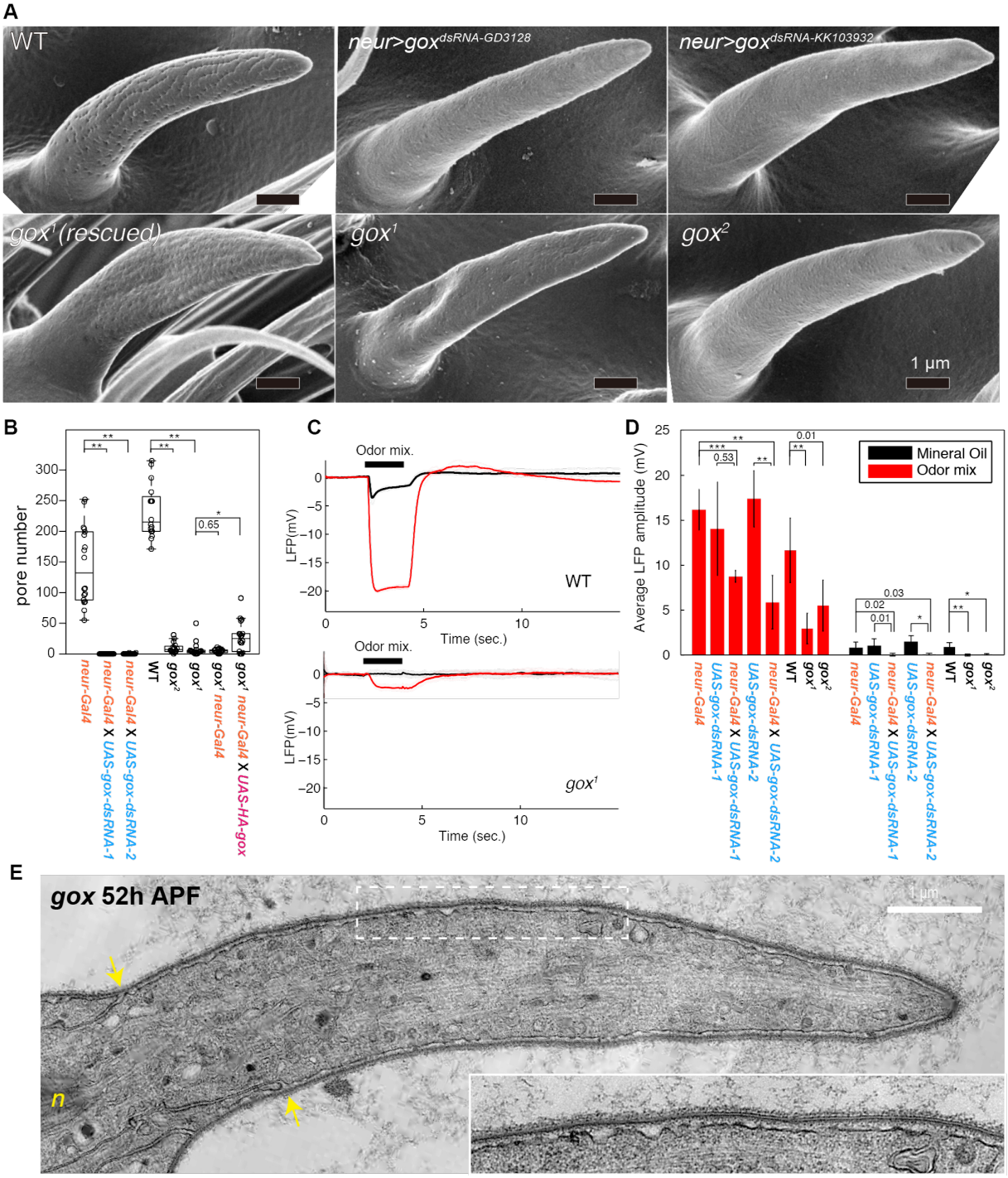

Fig. 2. Characterization of *gore-tex* gene function. (A) Surface views of adult olfactory sensilla. (B) Pore counts per sensillum. Statistical significance tested by Mann–Whitney U test with Bonferroni correction is indicated by * ($p < 0.05/7$) , ** ($p < 0.01/7$). Concrete p-values are indicated when they are statistically nonsignificant. (C) Recording of local field potential (LFP) in a maxillary palp upon the application of an odor mixture (red line) and solvent only (mineral

oil, black line). Solid lines are an average of 5 trials. (D) Quantification of the odor response measured from 6 recordings for each genotype. Statistical significance tested by Student's t-test with Bonferroni correction is indicated by * ($p < 0.05/12$), ** ($p < 0.01/12$) and *** ($p < 0.001/12$). Concrete p-values are indicated when they are statistically nonsignificant. (E) A TEM image of a *gox*^{1} olf at 52 h APF. Arrows indicate the boundaries between an olfctory shaft cell and adjacent epidermal cells. n: neurite.

Figure 3

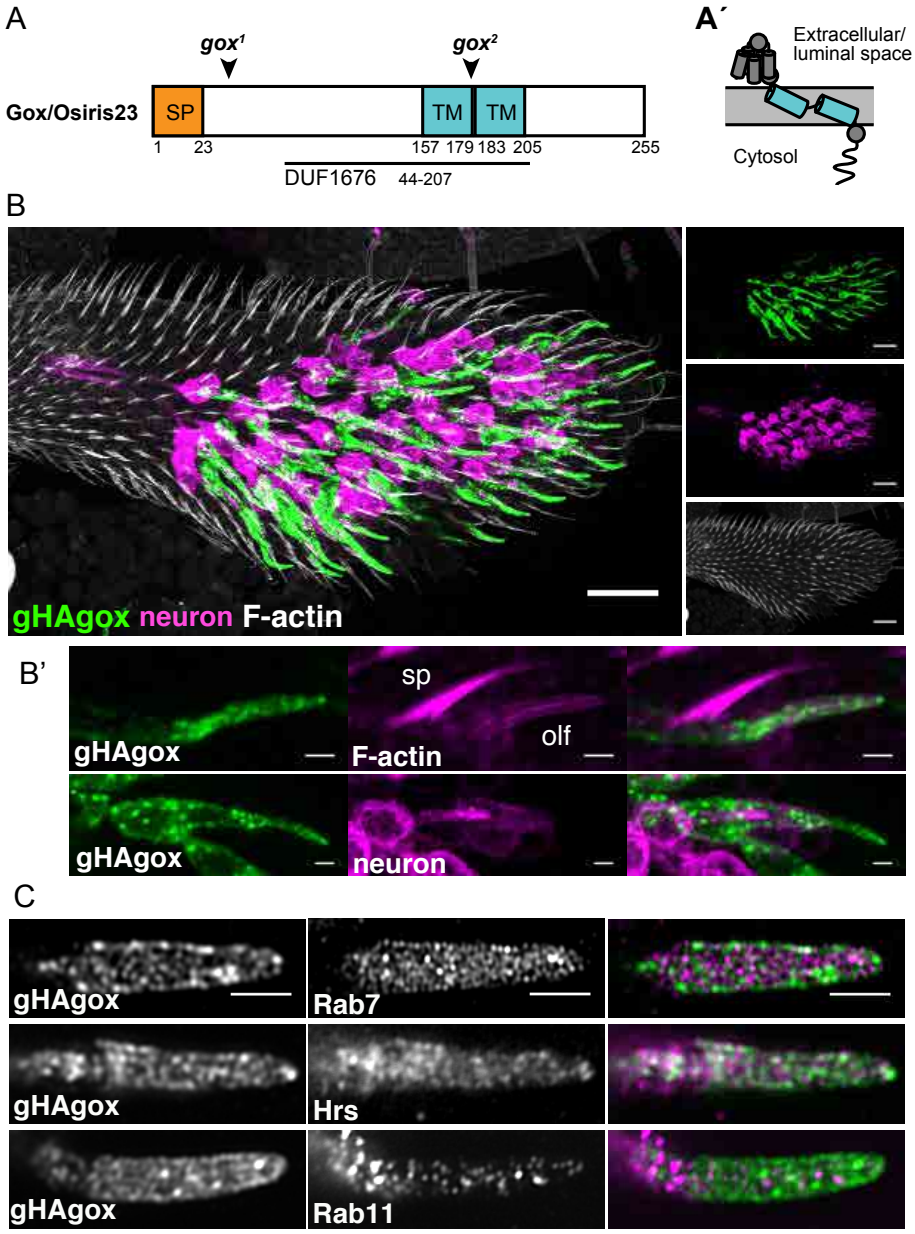

Fig. 3. Expression of Gore-tex protein. (A) A schematic diagram of the Gore-tex domain organization and predicted membrane topology. (B) Whole-mount staining of an mp at 44 h APF showing the expression of an HA-tagged genomic *gox* transgene, neurons, and F-actin staining. (B', B'') HA-*gox* is expressed in olf with a low level of F-action, and not in neurons that innervate into olf. (C) Subcellular localization of HA-Gox and organelle markers (Rab7, Hrs, Rab11). Scale bar: 10µm (B), 2 µm (B', C).

Figure 4

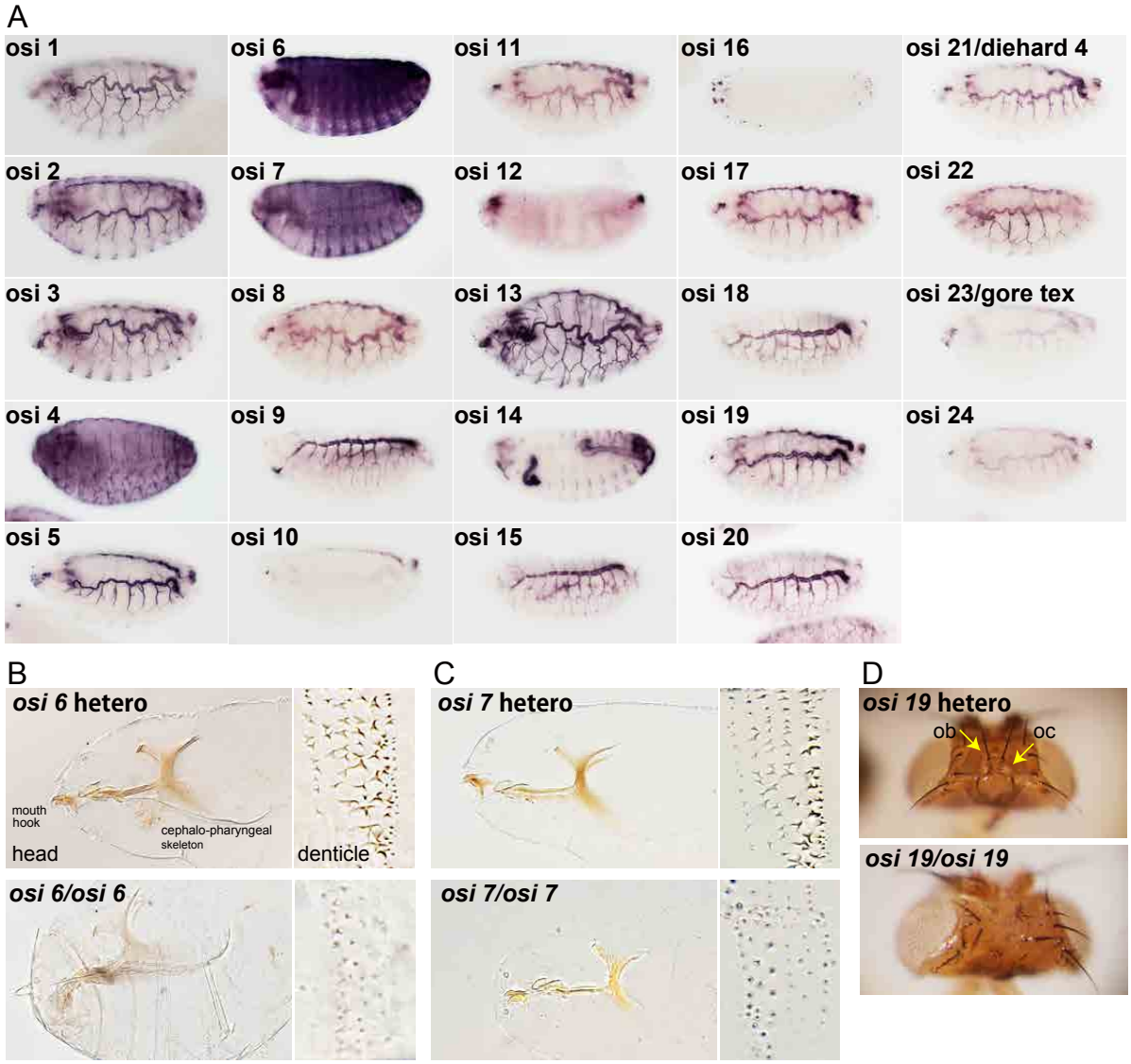

Fig. 4. Expression and function of the *Osiris* gene family. (A) Embryonic mRNA expression patterns of 24 *Osiris* genes. (B) *Osi6* mutant embryos. Images of heads (left) and denticle belts (right). (C) *Osi7* mutant first instar larvae. (D) Adult heads of *Osi19* mutants. Ocelli (oc) were missing, and orbital bristles (ob) were partially lost in homozygotes.